Journal Pre-proofs

Article

Designing non-hermitian real spectra through electrostatics

Russell Yang, Jun Wei Tan, Tommy Tai, Jin Ming Koh, Linhu Li, Stefano Longhi, Ching Hua Lee

PII: S2095-9273(22)00350-4
DOI: https://doi.org/10.1016/j.scib.2022.08.005
Reference: SCIB 1838

To appear in: *Science Bulletin*

Received Date: 12 March 2022
Revised Date: 29 June 2022
Accepted Date: 29 July 2022

Please cite this article as: R. Yang, J.W. Tan, T. Tai, J.M. Koh, L. Li, S. Longhi, C.H. Lee, Designing non-hermitian real spectra through electrostatics, *Science Bulletin* (2022), doi: https://doi.org/10.1016/j.scib.2022.08.005

Designing non-Hermitian real spectra through electrostatics

Russell Yang,[1,2,*] Jun Wei Tan,[3] Tommy Tai,[4] Jin Ming Koh,[5] Linhu Li,[6] Stefano Longhi,[7,8] and Ching Hua Lee[3,†]

[1]*Department of Physics, National University of Singapore, Singapore 117551, Republic of Singapore*
[2]*Clarendon Laboratory, University of Oxford, Oxford OX1 3PU, UK*
[3]*Department of Physics, National University of Singapore, Singapore 117551, Singapore*
[4]*Cavendish Laboratory, University of Cambridge, Cambridge CB3 0HE, UK*
[5]*Division of Physics, Mathematics and Astronomy, Caltech, Pasadena CA 91125, USA*
[6]*Guangdong Provincial Key Laboratory of Quantum Metrology and Sensing & School of Physics and Astronomy, Sun Yat-Sen University (Zhuhai Campus), Zhuhai 519082, China*
[7]*Dipartimento di Fisica, Politecnico di Milano, Piazza Leonardo da Vinci 32, I-20133 Milan, Italy*
[8]*IFISC (UIB-CSIC), Instituto de Fisica Interdisciplinary Sistemas Complejos - Palma de Mallorca, E-07122 Spain*

(Dated: August 2, 2022)

Non-hermiticity presents a vast newly opened territory that harbors new physics and applications such as lasing and sensing. However, only non-Hermitian systems with real eigenenergies are stable, and great efforts have been devoted in designing them through enforcing parity-time (PT) symmetry. In this work, we exploit a lesser-known dynamical mechanism for enforcing real-spectra, and develop a comprehensive and versatile approach for designing new classes of parent Hamiltonians with real spectra. Our design approach is based on a new electrostatics analogy for modified non-Hermitian bulk-boundary correspondence, where electrostatic charge corresponds to density of states and electric fields correspond to complex spectral flow. As such, Hamiltonians of any desired spectra and state localization profile can be reverse-engineered, particularly those without any guiding symmetry principles. By recasting the diagonalization of non-Hermitian Hamiltonians as a Poisson boundary value problem, our electrostatics analogy also transcends the gain/loss-induced compounding of floating-point errors in traditional numerical methods, thereby allowing access to far larger system sizes.

Keywords: Non-hermitian, Electrostatics, Bulk-boundary correspondence, Band structure engineering, Real spectrum, Non-Hermitian Skin effect

I. INTRODUCTION

Condensed matter physics has traditionally been studied in the Hermitian context, since real energies are necessary for observing stable quantum states. Yet, with intense recent research in non-Hermitian systems [1], it has become apparent that many of the most exciting contemporary phenomena – exceptional points [2–4], non-Hermitian skin localization and modified bulk-boundary correspondence [5–11], nontrivial spectral topology [12–18], negative entanglement entropy [19, 20], effective non-Hermitian curved spaces [21], amplified Rabi frequencies [22] – exist only in the non-Hermitian realm. Fortunately, non-Hermitian systems are not necessarily unstable, since they can still possess real eigenenergies if appropriately designed. To guarantee real spectra, a key approach has been to enforce parity-time (PT) symmetry [23–26], such that the gains and losses conspire to give rise to eigenstates with conserved total amplitude. However, it should be emphasized that having a PT symmetric Hamiltonian is neither a necessary nor a sufficient condition for obtaining real spectra - not sufficient because we also require the PT symmetry to be unbroken [27]. This additional condition restricts candidate non-Hermitian systems to particular optical media [28–31] or lattice configurations [32, 33], thereby forgoing potentially rich possibilities afforded by many other platforms [34–37]. On the other hand, PT symmetry is also not a necessary condition because pseudo-hermiticity provides a more definitive condition for real spectra [38, 39]. However, pseudo-Hermiticity exists in our context only in the a priori unknown engineered real spectrum system, and not the parent PBC Hamiltonian to be found.

All in all, this work is motivated by the lesser-known observation that even without PT symmetry, non-Hermitian gain/loss can still *dynamically* cancel in a bounded medium, if they enter through directed unbalanced couplings. In such cases, states moving in one direction will be amplified, while those moving in another direction will be attenuated. For a bounded system, these gain/loss processes cannot continue forever, and states become stable once they are "trapped" by a boundary. This mechanism thus constitutes an alternative approach to real energy spectra (pink region in Fig. 1a), in addition to PT symmetry and/or hermiticity. Indeed, such real spectra have been found in simple bounded non-Hermitian lattices with asymmetric nearest-neighbor couplings [40, 41]. However, generalizing this dynamical mechanism for real spectra to richer, more complicated lattices remains a challenge, since unbalanced couplings also destroy the cherished Bloch property associated with ordinary translation-invariant states, necessitating the

* russell.yang@chch.ox.ac.uk
† phylch@nus.edu.sg

additional knowledge of the generalized Brillouin zone (GBZ) [8, 42]. With the form of the GBZ being difficult to obtain analytically in all but the simplest cases [8, 42–45], the comprehensive design of systems with real non-Hermitian spectra thus hinges on a fundamentally more illuminating approach for treating the effects of unbalanced non-Hermitian couplings.

In this work, we circumvent these difficulties by developing a new electrostatics analogy that intuitively reconstructs parent Hamiltonians with desired spectra and spatial eigenstate profiles (Fig. 1b), different from known electrostatics analogies that related the correlations within complex non-Hermitian spectra with a Coulomb gas. This contrasts with conventional approaches where the Hamiltonian is fixed through a combination of symmetry arguments and empirical optimization, and the spectrum (desired or otherwise) subsequently computed from it. Being a reversal of conventional approaches, our electrostatics analogy also avoids directly diagonalizing non-Hermitian Hamiltonians, which usually suffers from fatal floating-point errors in large systems [42].

Our electrostatics analogy exploits the hitherto unexploited parallel between the conformal structure of electric field lines in real space, and the complex spectral flow as non-Hermitian states accumulate along boundaries (Fig. 1 and Table I). It identifies non-Hermitian periodic/open boundary condition (PBC/OBC) spectra respectively with the loci of grounded conductors and electrostatic charges. Their electrical potential distribution gives the corresponding extent of boundary state accumulation, a key property that stabilizes state evolution, with no Hermitian analog. As such, instead of having to solve complicated algebraic equations to determine the GBZ, one just needs to solve the equivalent electrostatics problem, i.e., the Poisson equation [46], which is more geometrically intuitive. In particular, given a set of available couplings, all possible non-Hermitian models with real OBC spectra can be obtained by solving the corresponding electrostatics problem with charges restricted to a line, and grounded conductors determined by the coupling constraints.

In the rest of this work, we first explain the mechanism of obtaining real spectra from unbalanced (asymmetric) couplings, and use that to develop our electrostatics analogy and design approach. Next, after two pedagogical warm-up examples with well-known models, we demonstrate how we can robustly discover new models with real spectra, even when unexpected from symmetry arguments. Finally, we discuss our electrostatics reconstruction beyond the context of real spectra, where it is equally mathematically valid, and still physically relevant either as an optimization avenue, or in the context of network Laplacians.

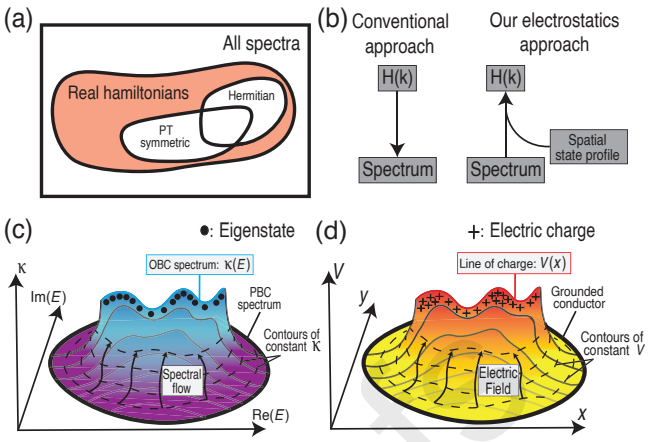

FIG. 1: (Color online) **(a)** Hermiticity and PT-symmetry are two well-known routes towards real energy spectra, but our work provides a new approach for designing generic real-spectrum Hamiltonians (pink) satisfying neither condition. **(b)** Conventionally, model Hamiltonian parameters have to be repeatedly optimized to yield the desired spectrum. By contrast, our electrostatics design approach directly outputs a parent Hamiltonian H possessing almost any desired eigenspectrum and eigenstate profiles. **(c)** Non-Hermitian eigenstates are characterized by their complex energies E and inverse spatial decay lengths κ, which together describe a landscape $\kappa(E)$. In particular, PBC eigenstates lie along $\kappa = 0$ loops, while OBC eigenstates accumulate along ridges where $\kappa(E)$ is not smooth. **(d)** The $\kappa(E)$ landscape of a non-Hermitian system is mathematically equivalent to the $V(x, y)$ potential landscape of its electrostatics analog, with PBC and OBC spectral loci corresponding to grounded conductors ($V = 0$) and lines of induced charges respectively. See Tables I, Sect. II and the Supplementary materials Sections I, II, III, and IV for more elaboration.

II. UNBALANCED COUPLINGS, REAL SPECTRA AND THEIR ELECTROSTATICS ANALOGY

Before deriving our electrostatics analogy, we first recap how unbalanced non-Hermitian couplings can lead to real spectra and hence stable eigenstates. Non-Hermitian systems that possess real spectra experience nontrivial gain and loss, but their effects balance out such that states do not grow or decay indefinitely, whilst retaining novel non-Hermitian properties. Unlike the conventional route of attaining this balance through certain global symmetries, i.e., PT symmetry, we shall consider a less known *dynamical* balance approach via unbalanced couplings between lattice sites in a bounded lattice. Away from boundaries (more generally, spatial inhomogeneities like disorder or impurities), unbalanced couplings cause

states to grow or decay unimpeded while moving in different directions, resulting in eigenenergies with negative/positive imaginary parts. However, since amplification/decay is tied to spatial motion, further amplification of wavepackets is inevitably resisted upon reaching a boundary, resulting in boundary-accumulated skin states. If this resistance to amplification is perfect, the spectrum will become real.

The simplest example is given by the Hatano-Nelson model [40]

$$H_{\mathrm{HN}} = \sum_j t_+ c_j^\dagger c_{j+1} + t_- c_{j+1}^\dagger c_j \tag{1}$$

with unequal nearest neighbor couplings $|t_+| \neq |t_-|$ only. Without boundaries(PBCs), amplification is unimpeded and its PBC spectrum is complex, given by $E_{\mathrm{HN}} = t_+ e^{-ik} + t_- e^{ik}$, $k \in [0, 2\pi)$. However, in the presence of a boundary, its OBC spectrum $\bar{E}_{\mathrm{HN}} = 2\sqrt{t_+ t_-}\cos k$ is real [43] due to non-Bloch boundary accumulation $\psi(x) \sim \psi(x)\,(t_+/t_-)^x$ which induces $k \to k + i\log\sqrt{\frac{t_-}{t_+}}$. While it is straightforward to understand the perfect balance of gain/loss in this particular simple model, boundaries induce a very complicated deformation $k \to p(k) = k + i\kappa(k)$ in most other models, i.e., the OBC spectrum $\bar{E}$ converges towards a complex momentum deformation of the PBC spectrum $E(k)$, i.e., $\bar{E}(k) = E(k + i\kappa(k))$ [6], as elaborated in the Supplementary materials Section I. As a complex extension of the Bloch momentum, $\kappa(k)$ corresponds to real-space decay, and is known as the inverse skin depth of the k-eigenstate. Mathematically, $\kappa(k)$ must satisfy the condition that there exist at least two different k, k' such that $\bar{E}(k) = \bar{E}(k')$ and $\kappa(k) = \kappa(k')$. Such conditions can be expressed as a rather complicated singular function, which is in general difficult to solve.

Alternatively, our electrostatics approach sheds geometric intuition to the rather opaque algebraic problem of finding non-Hermitian OBC spectra, and provides a more intuitive and tractable approach for engineering the most generic lattice Hamiltonians with real spectra. To understand how, note that the complex deformation $k \to p(k)$ can be understood geometrically (Fig. 1c): While the PBC spectrum (solid loop) traces out a loop $E(k)$, $k \in [0, 2\pi)$ in the complex E plane, the OBC spectrum (line of crests within the loop) is obtained by the ramping up $|\mathrm{Im}(p)|$ such that the PBC loop "shrinks" into its interior until it overlaps with itself, i.e., is degenerate everywhere [6, 15, 47, 48]. In this OBC limit, the spectrum $\bar{E}$ traces out lines or curve segments connected to each other at branch points. In particular, the OBC spectrum is real if the PBC loop successfully shrinks into a segment on the real line. Our electrostatics approach below shows that this can be achieved/engineered no matter how complicated the PBC Hamiltonian is.

To connect with electrostatics (Fig. 1d), we turn to the conformal mapping $p(E)$, which is the inverse of the complex energy dispersion, the momentum p and energy E both regarded as complex variables. The analog of $p(E)$ in electrostatics is the quantity $\phi(z)$, where $z = x + iy$ represents real space, and curves of constant $U = \mathrm{Re}(\phi)$ and $V = \mathrm{Im}(\phi)$ represent field lines and equipotentials respectively. Corresponding to them are curves of constant $\mathrm{Re}(p) = k$ and $\mathrm{Im}(p) = \kappa$ respectively (Table I). Fig. 1 compares the profile of the inverse skin depth $\kappa(E)$ with its analog, the electrical potential $V(z)$. Intuitively, we make this correspondence since any conformal map, by definition, must preserve the orthogonal nature of the field lines and equipotentials. Likewise, unique isolines in the skin depth $\mathrm{Im}(p) = \kappa$ remain orthogonal to lines of constant $\mathrm{Re}(p) = k$ under adiabatic OBC-PBC transformation in steps of constant κ [43]. It should be noted that this electrostatics analogy relating the non-Hermitian skin effect problem to electrostatics is unrelated to other electrostatic analogies concerning the spectra of random non-Hermitian matrices [49–51], where the Green's function is found to have a $1/r$ dependence resembling the Coulomb electrostatic potential. In these works, the eigenvalue correlations are found to resemble that of a Coulomb gas, while in our analogy, it is the complex spectral flow that is found to contain the conformal structure of an equipotential vs. electric field lines pair.

In addition, it is quite straightforward to associate grounded conductors, i.e., contours of constant $V = \mathrm{Im}(\phi) = 0$ with PBC eigenenergy loops $E(k)$, $k \in [0, 2\pi)$ (solid closed loops in Fig. 1c, d). This is because $\mathrm{Im}(p) = \kappa = 0$ for PBC Bloch eigenstates, due to their translation invariance. However, the OBC eigenenergies $\bar{E}(k) = E(k + i\kappa(k))$ do not in general correspond to any equipotential, unless $\kappa(k)$ happens to be constant. Instead, we identify the OBC spectra with regions of nonzero electric charge, since they are precisely where solution surfaces $\kappa(E)$ intersect (crests within the loops in Fig. 1c, d), such that the corresponding potential surfaces $V(z)$ become piecewise continuous. Specifically, nonzero electrical charge density $\varepsilon_0 \nabla_z^2 V$ is inherited from the nonzero $\nabla_E^2 \kappa \neq 0$ at these crests.

What makes this electrostatics analogy particularly useful is that the density of states (DOS) in the non-Hermitian system corresponds to the charge density in the electrostatic problem. As such, an electrostatic solution (of the Poisson equation) can be used as a proxy for solving the equivalent non-Hermitian problem, whose numerical diagonalization may be undesirably sensitive to noise. To understand this duality between charge density and spectral density, note that the DOS along an arbitrary curve ϵ in the complex E plane of a lattice with L sites is given by

$$\rho_\epsilon = \frac{L}{2\pi}|\hat{\epsilon} \cdot \nabla_E(k)| = \frac{L}{2\pi}|\hat{\epsilon} \times \nabla_E(\kappa(k))|, \tag{2}$$

since there are L eigenstates along a loop $E(p)$ parametrized by $\mathrm{Re}(p) = k \in [0, 2\pi)$, with fixed $\mathrm{Im}(p)$ chosen such that the loop intersects ϵ. Here E and and the unit tangent vector $\hat{\epsilon} = \epsilon/|\epsilon|$ are treated as 2D vectors. The second equality was obtained via the Cauchy-

TABLE I: Correspondence between a non-Hermitian lattice and its electrostatic analogy.

Non-Hermitian lattice	**Electrostatic system**	**Remarks**
Complex energy E [a]	Complex position $z = x + iy$ [a]	
Inverse skin depth/ imaginary flux $\kappa(E)$ [a,b]	Electrical potential $V(z)$ [a,b]	Specified as input along the OBC spectrum
Density of states ρ_ϵ [c]	Electrostatic charge density σ_ϵ [c]	Nonzero along the OBC and PBC spectra
OBC to PBC spectral interpolation curve	Electric field lines of const. $U(z)$	
PBC spectrum $E(k)$	Grounded conductor $\epsilon^{\mathrm{PBC}}(U)$	Specified as input
OBC spectrum $E(k + i\kappa)$ [d]	Path of nonzero charge density	Specified as input

[a]These quantities are of primary importance as they completely define their respective systems. [b]Analogous to the electrical potential V is the skin depth κ^{-1} of accumulated states arising from the unbalanced non-Hermitian hoppings. [c]ϵ refers to a generic path on the complex energy (spatial) plane E (z), emphasizing that σ_ϵ and ρ_ϵ are in principle proportional along any curve, not just the real line. [d]Whether the OBC spectrum $\bar{E}(k) = E(k + i\kappa)$ can be real depends on whether the Poisson equation on V is consistent with nonzero charge density σ_ϵ only along $y = 0$, i.e., nonvanishing spectral density of states (DOS) ρ_ϵ along $\mathrm{Im}(E) = 0$.

Riemann relations. According to our electrostatics analogy, $\kappa = \mathrm{Im}(p)$ correspond to the electrical potential V, and $\nabla_E(\kappa)$ thus corresponds to the negative electric field strength $-\mathcal{E} = \nabla V$. Along a path ϵ such that there is a discontinuity in the field strength, the induced charge density can be shown via a Gaussian pillbox to be

$$\sigma_\epsilon = \mp 2\varepsilon_0 |\hat{\epsilon} \times \nabla V|, \tag{3}$$

where ε_0 is the permittivity of the medium, and the sign of $\mp$ dependent on the direction of the discontinuity step. Evidently, then, the charge and corresponding spectral densities are proportional, $\sigma_\epsilon \propto \rho_\epsilon$, with the proportionality constant fixed by the constraint that the total number of states in the entire spectrum is L.

Some comments are in order regarding the discreteness of the charges. So far, in formulating the electrostatics analogy, we have tacitly assumed large L, such that the DOS and hence their corresponding charge density tends towards a continuum. However, there exist scenarios of non-Bloch band collapse [52, 53], where there exists couplings towards only one uncompensated direction, and the OBC spectrum shrinks into one of more isolated $\bar{E}$ points, with divergent κ and hence V. Such scenarios exactly correspond to electrostatic problems with isolated point charges, which include extremely well-understood textbook examples. As elaborated in Supplementary materials Section V, classic approaches such as the method of Images and superposition of point charges allow for the elegant design of Hamiltonians exhibiting non-Bloch band collapse onto an arbitrary variety of point charge configurations.

III. DESIGNING HAMILTONIANS WITH DESIRED SPECTRA VIA ELECTROSTATICS

We now elaborate on how our electrostatics analogy can help us engineer realistic Hamiltonians that possess desired OBC eigenenergies, particularly real eigenenergies. Conventionally, as indicated in Fig. 1b, given a lattice Hamiltonian $H(k)$ with known properties, i.e., topological properties, one simply computes its OBC or PBC spectrum by numerical diagonalization under the respective boundary conditions. However, even though it is easy to write down a Hamiltonian $H(k)$ that gives rise to a particular PBC spectrum $E(k)$, it is much more nontrivial to design a $H(k)$ that gives a desired OBC spectrum $\bar{E}(k) = E(k + i\kappa(k))$, since $\kappa(k)$ usually takes a very complicated form. Yet, it is the OBC spectrum that holds the key to achieving real spectra beyond the symmetry constraint paradigm.

Our electrostatics analogy is tailor-fit to solve this inverse problem of finding $H(k)$ with desired OBC spectral properties. Based on Table I and surrounding discussions, the key input specifications for the desired OBC states are exactly the crucial data for constructing the electrostatic analog. Namely, they are

(i) the locus of the desired OBC spectrum in the complex E plane, which specifies the locations of the analog electrostatic charges,

(ii) the desired spatial profile (skin depth κ) of its eigenstates, which specifies the electrical potentials at their analog charges, and

(iii) the shape of the desired PBC spectrum.

As illustrated in Fig. 1, the OBC eigenvalues/charges manifest as ridges, and (i) and (ii) respectively give the positions and heights of these ridges. To uniquely define the electrostatic system, we additionally specify the boundary equipotentials that enclose these ridges, which correspond to (iii) the shape of the desired PBC spectrum.

Combined together, these data are sufficient for determining the electrostatic potential $V(z)$ everywhere, and ultimately recovering the parent $H(k)$ that produces them. This can be achieved through the following workflow, whose conceptual and implementation details are elaborated in the Supplementary materials Section III. First, we obtain $V(z)$ everywhere by solving the Poisson

equation with respect to Dirichlet boundary conditions from stipulated input data (i) to (iii). Next, by applying Gauss's law on $\mathcal{E} = -\nabla V$, we obtain the induced charges on the boundary conductor, which corresponds to the PBC spectral locus. Due to the proportionality between electrostatic charge σ and its corresponding spectral density ρ (Eqs. 2 and 3), we hence obtain the DOS along the PBC curve stipulated by input (iii). As illustrated in Fig. 2a, this determines the k-point spacing along the PBC curve, leading to a full reconstruction of $E(k)$ and hence $H(k)$ as further described in the Supplementary materials Section III. With a known candidate $H(k)$, the real-space couplings can be obtained via Fourier transformation.

For more insight into the motivation behind our approach, it is instructive to contrast generic non-Hermitian scenarios with Hermitian scenarios. In the latter, the PBC and OBC spectra are both real, and largely overlap except possibly at isolated points. Hence their potential surfaces in Fig. 1c, d would have been compressed onto the real E line. This forces inputs (i) and (iii) to the same line segment on the real line. Furthermore, Hermitian eigenstates are Bloch states with $\kappa = 0$, so input (ii) would have been moot, with the electrostatic setup reducing to a trivial equipotential line, instead of a potential surface in the 2D plane. At a deeper level, our electrostatics approach reinforces that even if two non-Hermitian lattice systems possess the same OBC spectra, they can still differ in two fundamentally independent aspects: their (ii) eigenstate skin depths κ and (iii) PBC spectra.

Before presenting new Hamiltonians designed with our approach, we shall first provide two pedagogical illustrations using familiar non-Hermitian models—the Hatano-Nelson model [40] and the non-Hermitian SSH model [5, 54]. Both models are already known to possess real OBC spectra due to unbalanced directed gain/loss, not symmetry protection, since the same models under PBCs do not have real spectra. However, for the purpose of illustration, we shall assume no *a priori* knowledge of these models, and derive their Hamiltonians based on the input data (i) to (iii) discussed earlier: to recap, (i) range of the desired real OBC spectra, (ii) desired skin depths κ^{-1} of their corresponding OBC states, and (iii) complex paths traced out by their PBC spectra, which uniquely specifies the possible output models.

A. Warm-up I: Hatano-Nelson model

In this simplest first example, we show how the HN model (Eq. (1)) can be recovered just from stipulating its real OBC spectrum, uniform κ and elliptical PBC spectral locus. From the previous subsection, its OBC eigenenergies lie along the real segment $\bar{E}_{\rm HN} \in [-2\sqrt{t_+t_-}, 2\sqrt{t_+t_-}]$, and the PBC eigenenergies $E_{\rm HN}$ are distributed along an ellipse with semi-major/minor axes $t_+ \pm t_-$ in the complex plane (Fig. 2b). Note that we have *not* parametrized both the OBC and PBC spectra, because the DOS and hence functional forms of these spectra are *a priori* unknown. We also stipulate that all OBC eigenstates have similar spatial decay profiles, i.e., uniform κ in anticipation of recovering the HN model; different distributions of $\kappa(E)$ can lead to very different parent Hamiltonians, albeit with identical OBC and PBC spectral loci.

In Fig. 2b, these stipulated OBC and PBC spectra are mapped onto an electrostatic system with a real line segment $x \in [-2\sqrt{t_+t_-}, 2\sqrt{t_+t_-}]$ (blue) of elevated uniform potential $V = \log\sqrt{t_-/t_+}$ enclosed by an elliptical equipotential $V = 0$ (black) with semi-major/minor axes $t_+ \pm t_-$. The Laplace equation on this boundary-value problem possesses an analytic solution $V(z) = -\log|(z \pm \sqrt{z^2 - 4t_+t_-})/2t_-|$, the $\pm$ sign depending on $\mathrm{sgn}[x(t_- - t_+)]$. This gives precisely the functional form of $V = \mathrm{Im}(p)$ in the (complexified) energy dispersion $E_{\rm HN}(p) = z$, establishing that energy $E = E_{\rm HN}$ indeed corresponds to the position z in this analogy, and that $H_{\rm HN}$ is indeed the parent Hamiltonian that yields these stipulated specifications on the spectrum and κ.

B. Warm-up II: non-Hermitian SSH model

We next show how a more complicated 2-component parent Hamiltonian can be recovered via our approach without the benefit of a known analytic solution. As a warm-up demonstration, the stipulated spectral loci are based on the known non-Hermitian SSH model [5, 54] $H_{\rm SSH}$, even though the model itself is assumed to be *a priori* unknown, and meant to be reconstructed. In this case, the real spectrum $\bar{E}_{\rm SSH}$ is specified to lie within the two real segments $1 - T < |\mathrm{Re}(E)| < 1 + T$, corresponding to the segments of constant elevated potential V in the z plane of the electrostatic analog (Fig. 2c). They are enclosed by a grounded ($V = 0$) outer boundary corresponding to the PBC locus of $E_{\rm SSH}$, which we stipulate (with the benefit of hindsight, for illustration purposes) as

$$\gamma^2(x^2 - y^2 + \gamma^2 - 1 - t^2)^2 = 4t^2(\gamma^2 - x^2y^2), \quad (4)$$

γ and $t = \sqrt{T^2 + \gamma^2}$ parameters of the $H_{\rm SSH}$ to be found. Spatial coordinates (x, y) correspond to the spectral locus $(\mathrm{Re}(E_{\rm SSH}), \mathrm{Im}(E_{\rm SSH}))$. We emphasize that specifying the locus of $E_{\rm SSH}$ does not imply knowledge of either the PBC spectrum $E_{\rm SSH}(k)$ or its Hamiltonian $H_{\rm SSH}(k)$, since the parametrization with k is still unknown.

For a model with 2 or more components, obtaining a physically realistic Hamiltonian $H(k)$ from the dispersion $E(k)$ via $\mathrm{Det}[H(k) - E(k)\mathbb{I}] = 0$ presents an additional avenue of subtlety. As there are many possible forms of $H(k)$ which all yield the same eigenenergy $E(k)$, it is crucial to choose a correct ansatz that allows all components of $H(k)$ to possesses rapidly decaying Fourier

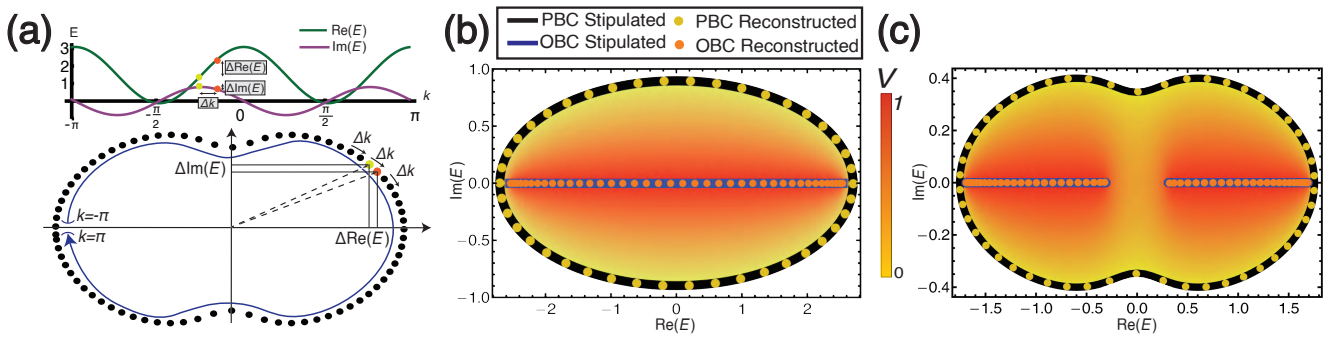

FIG. 2: (Color online) **Exact agreement between the stipulated and reconstructed spectra in our design approach, for the two warm-up models.** **(a)** The spectrum $E(k)$ of the output Hamiltonian is reconstructed by setting energy intervals ΔE between equal momentum spacings Δk to be inversely proportional to the density of states ρ_ϵ, which is obtained from the induced charge density σ_ϵ in the equivalent electrostatic problem. **(b)** Warm-up example I with stipulated OBC spectrum on the real line segment $|x| \leq 2\sqrt{t_+ t_-}$ with constant eigenstate decay profile κ^{-1}, corresponding to a constant electrical potential V. Its elliptical PBC spectral locus corresponds to a grounded conductor, giving rise to induced charges that enable the reconstruction of the full Hamiltonian $H_{\rm HN}(k)$. As a check, its PBC and OBC spectra fall exactly on the initially stipulated loci. Parameters used are $t_+ = 0.9$, $t_- = 1.8$ and $n = 42$ lattice sites. **(c)** Warm-up example II with two stipulated real OBC line segments, PBC locus of the form of Eq. (4) and constant κ. The corresponding electrical potential induces charges that allow the reconstruction of an $E_{\rm SSH}(k)$ dispersion, corresponding to the 2-component $H_{\rm SSH}(k)$ from Eq. (5) with parameters $\gamma = 0.4$, $t = 0.8$ and $n = 50$ sites. Both the PBC and OBC spectra of $H_{\rm SSH}$ display perfect agreement with their initially stipulated loci. Note that we have normalized the potential to $V = 1$ along the real line segments in both **b** and **c**.

coefficients, such that the solution corresponds to a local Hamiltonian. In general, the Fourier coefficients f_x of a function $f(k)$ decay like $f_x \sim x^{-(1+\beta)} e^{-\eta x}$, where η is the distance between the real line and the nearest complex singularity of $f(k)$ and β, the order of that singularity, which is either negative or fractional. That is, $f(k + i\eta) \approx (k - k_0)^\beta + f_0$, with k_0 and f_0 being constants [55, 56]. In particular, local Hamiltonians should possess $\eta > 0$, which means $H(k)$ should not contain divergences or branch points at $k \in \mathbb{R}$.

In this case, the reconstructed PBC dispersion can be fitted to the square-root expression $E_{\rm SSH}(k) = \pm\sqrt{1 + 2t\cos k + T^2 + 2i\gamma \sin k}$, which will result in unphysical long-ranged hoppings if we use a 1-component ansatz Hamiltonian. But since $E^2_{\rm SSH}(k)$ does not contain branch cuts, a prudent choice would be a 2-component ansatz Hamiltonian with only off-diagonal elements (see Supplementary materials Section III), which can be shown to be

$$H_{\rm SSH}(k) = (t + \cos k)\sigma_x + (\sin k + i\gamma)\sigma_y. \qquad (5)$$

Shown in Fig. 2c is the excellent match between the OBC/PBC spectra of the reconstructed $H_{\rm SSH}$ (orange/yellow), compared with the initially stipulated elevated potential interval along the real line (blue) and the boundary equipotential (black). This is one of the very few models where a constant κ deformation, i.e., potential V, can recover a real OBC spectrum—specifically, $k \to p = k + i\kappa$ where $\kappa = \log[(t + \gamma)/(t - \gamma)]/2$, such that $\bar{E}_{\rm SSH}(k) = E_{\rm SSH}(p) = \pm\sqrt{1 + 2T\cos k + T^2}$ is real when $|t| > |\gamma|$. In the following, we shall explore how, by varying the PBC spectral locus and the $\kappa(E)$ profile for OBC states, we can engineer a much greater variety of hitherto undiscovered models with real spectra.

C. Real OBC states with non-constant skin depths κ^{-1}

We now turn to the first nontrivial demonstration of our approach, where we design a Hamiltonian stipulated to possess an OBC spectrum occupying two real line segments, each with a different value of κ. Consider the spectra shown in Fig. 3a, which naively looks like a simple variant of the Hatano-Nelson or SSH model, with specified OBC real line segments lying symmetrically about the origin, surrounded by an also symmetric elliptical PBC spectral locus. However, what is nontrivially asymmetric is the unequal inverse skin depth κ (corresponding to V) of the eigenstates lying on each line segment, which cannot be fulfilled via any simple extension of these models. As a property with no Hermitian analog, κ is entrenched in the complex analytic properties of the Hamiltonian, and it is nontrivial to tune it without also modifying the spectrum. This is when our electrostatics analogy becomes valuable: corresponding to κ is the electrical potential V, and the task is reduced to that of solving the Laplace equation, subject to these $V = 1$ and $V = 1.6$ segments and the $V = 0$ outer boundary.

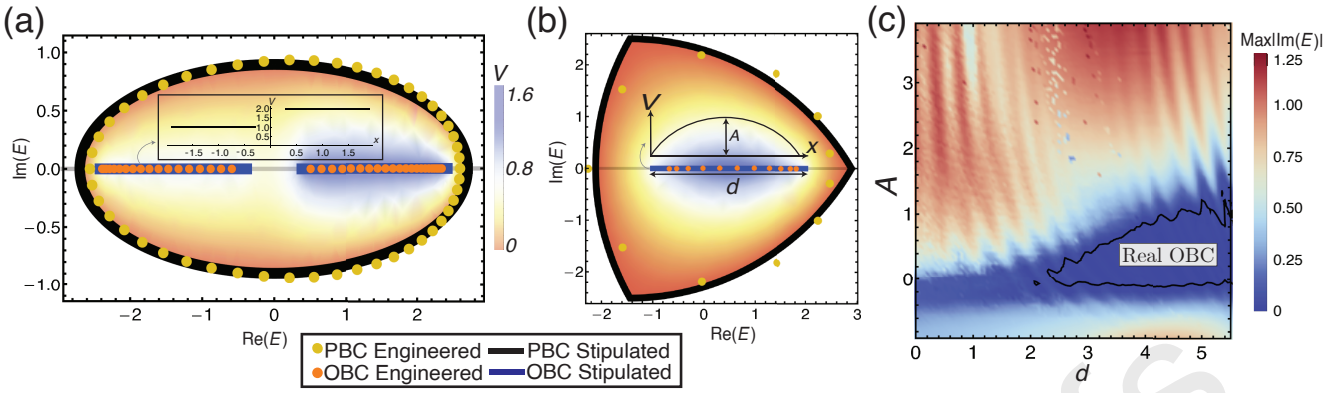

FIG. 3: (Color online) **Illustrative examples demonstrating a search for real-spectra parent Hamiltonians in nontrivial settings without special symmetries.** **(a)** PBC ellipse with two real OBC segments with unequal skin depths: the stipulated real OBC segments $\pm E \in [0.3, 2.4]$ are of asymmetrically different skin depths $\kappa^{-1} = 1$ and $1/2$, corresponding to potentials $V = 1$ and 1.6. Together with grounded conductors defined by the stipulated PBC spectral locus $(\mathrm{Re}(E)/2.7)^2 + (\mathrm{Im}(E)/0.9)^2 = 1$, they define an electrostatic problem, yielding a parent Hamiltonian in the form of Eq. (6). **(b)** PBC Reuleaux triangle with real OBC segment of length d and position offset $x_0 = -1$, with inhomogeneous skin depths corresponding to a concave potential $V(x)$ of amplitude A (Eq. (8)). Engineered (dotted) and stipulated (solid) spectra agree well, even though the engineered Hamiltonian is single-component with only up to next-nearest neighbor hoppings. **(c)** Values of $\mathrm{Max}|\mathrm{Im}(E)|$ for the OBC spectrum of our engineered Hamiltonian in the parameter space of A and d. There exists a large parameter region (blue) with almost real OBC, which is not expected given the very different symmetries of the Reuleaux triangle and the $V(x)$ profile. Tolerance for reality is $\mathrm{Max}|\mathrm{Im}(E)| \leq 0.02$, and 20 sites are used.

Upon solving this electrostatic problem and reconstructing the corresponding dispersion $E(k)$, we find that $E(k)$ has a slowly decaying train of Fourier components, and cannot result from a single-component local Hamiltonian. As discussed in the previous subsection, this is generically expected, and a resolving strategy is to consider an engineered Hamiltonian with 2 or more components (bands). To accommodate the asymmetry, we generalize the previous 2-component ansatz to:

$$H(k) = H_z(k)\sigma_z + T(k)\mathbb{I} + \mathcal{F}(k)\sigma_+ + \sigma_-, \qquad (6)$$

where $\sigma_\pm = (\sigma_x \pm i\sigma_y)/2$, which allows the reconstructed energy dispersion $E(k)$ to be fitted to either branch of the expression

$$E(k) = T(k) \pm \sqrt{\mathcal{F}(k) + H_z(k)^2}, \qquad (7)$$

where $T(k)$, $H_z(k)$ and $\mathcal{F}(k)$ each contain no more than a few Fourier components. The details of the fitting and solution branch selection are given in the Supplementary materials Section IV.

Showcased in Fig. 3a is the very good agreement between the PBC and the OBC spectra of the engineered Hamiltonian, compared to their stipulated counterparts. For this example, up to next-nearest neighbor hoppings were kept in H (see Supplementary materials Section VI); even better agreement and reality of spectra can obtained with further hoppings. Notice the unequal eigenenergy spacings between the left and right halves, which result "naturally" as induced charges from the asymmetric electrical potential (pale orange-purple). This asymmetric example also illustrates the distinction between the PBC dispersion $E(k)$ and the PBC spectral locus, which is the ellipse that is initially specified. Even though the latter is known *a priori*, the actual dispersion and density of states, which is skewed to the right as shown in Fig. 3a, can only be known after the potential profile $V(x, y)$, i.e., $\kappa(E)$, has been solved for. Graphically, it is also evident that steeper potential gradients lead to stronger induced charges and hence DOS on the right half. In the Supplementary materials Section VII, it is shown that good agreement was obtained not just for the stipulated and engineered spectra, but also for the $\kappa(\mathrm{Re}(E))$ profile, which corresponds to the $V(x)$ potential.

IV. REAL SPECTRA WITHOUT ANY SYMMETRY

Even though our electrostatics approach can in principle generate a parent Hamiltonian corresponding to any desired spectral loci and skin depth profiles, the usefulness of the reconstructed Hamiltonian hinges on its experimental feasibility. As such, it is oftentimes preferable to restrict the reconstructed Hamiltonians to a small number of relatively local real-space hoppings. With further hoppings truncated, the compromise is that the reconstructed spectra may no longer be exactly real, even though the stipulated desired spectra lie along the real line. Even then, our approach allows for a systematic exploration of the region in parameter space where a class

of local hopping models possesses almost real spectra, unaided by any specific symmetry.

As a demonstration, consider the rather demanding scenario where the desired PBC spectrum is stipulated along a so-called Reuleaux triangle (Fig. 3b), which is parametrically defined by the expression $E_{\text{Reuleaux}}(t) = \sqrt{3}e^{\frac{1}{6}i\left(2\pi\left\lfloor\frac{3t}{2\pi}\right\rfloor+3t+\pi\right)} - e^{\frac{1}{3}i\pi\left(2\left\lfloor\frac{3t}{2\pi}\right\rfloor+1\right)}$, $t \in [0, 2\pi)$. Such a shape has 3-fold rotational symmetry about the complex origin, which generically do not encourage real OBC spectra. Meanwhile, the stipulated OBC spectral locus is set to be a segment of length d along the real line $x \in (-1, 2)$, although it remains to be seen how faithfully the reconstructed OBC spectrum can reproduce this. As an additional complication, $\kappa(\text{Re}(E))$ (which corresponds to potential $V(x)$) is set to

$$V(x) = 1 + A \sin\left[\frac{\pi(x - x_0)}{d - x_0}\right] \tag{8}$$

with offset $x_0 = -1$ for definiteness, and A, d parameters to be tuned. We proceed as in the previous examples, and is able to obtain local and simple Hamiltonians that produce almost exactly real OBC spectra while respecting the stipulated inputs of this problem. For instance, the spectra showcased in Fig. 3b arose from the engineered Hamiltonian

$$H = \sum_j 0.613c_j^\dagger c_j - 2.18c_j^\dagger c_{j+1} - 0.193c_{j+1}^\dagger c_j - 0.5c_j^\dagger c_{j+2} \tag{9}$$

whose real spectrum possess eigenstate localization profiles closely obeying $V(x)$, despite hoppings with no apparent symmetry whatsoever that even suggests of the possibility of a real spectrum. Containing only up to next-nearest neighbor hoppings, it is simple enough to realize in photonic systems given recent developments in the capability to control long range hoppings [57–59]. Mechanical and ultracold atomic systems also provide lee ways into implementing such systems [60, 61]. But perhaps the most versatile means is mechanical or electrical systems where hoppings of arbitrary order can be generated with appropriate circuit configurations [35, 62, 63].

The propensity of real spectra can be increased by optimizing parameters A and d. Shown in Fig. 3c is the value of OBC Max|Im(E)| in the parameter space of A and d, with hoppings across up to 5 sites. In general, although the reconstructed OBC spectra are not always perfectly real, they are still mostly real with "branches" pointing away from the real line (Fig. S3 online). Notably, there exists a large parameter region (purple) where the OBC spectrum is almost perfectly real, with Im(E) at least two orders of magnitude smaller than Re(E). Examples of almost-real spectra at different points in the parameter space can be found in the Supplementary materials Section VIII.

It is remarkable that this Hamiltonian can possess any real OBC spectrum at all, given that it not only lacks suitable conventional symmetry such as hermiticity or PT-symmetry, but also lacks any other ostensible symmetry that can encourage PBC→OBC spectral flow towards the real line.

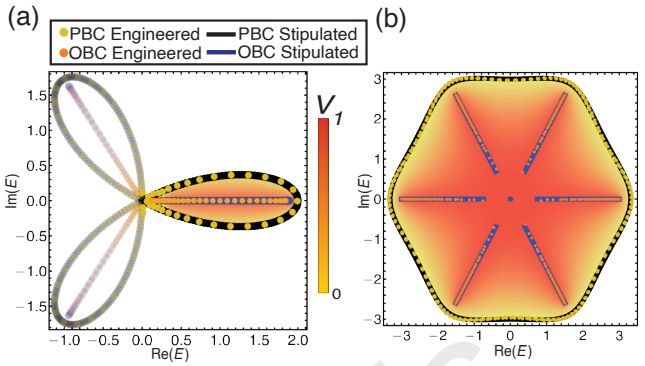

FIG. 4: (Color online) **Designing beyond real spectra.** **(a)** Almost perfect agreement between the stipulated and engineered spectra in the right lobe was achieved, with only up to next-nearest neighbor hoppings, by discarding solutions from the two other extraneous lobes. The stipulated PBC spectrum is given by the parametrization Eq. (10). **(b)** Excellent reconstruction can also be achieved by enlarging the number of components of the ansatz Hamiltonian and its solution branches. Here, the 3-component ansatz $H_{6\text{-fold}}$ (Eq. (13)) with $\Delta = 0$ allows for an excellent local fitting of $E(k)^3$ with minimal Fourier components. Stipulated OBC and PBC spectra are given by Eqs. 11 and 12, with $r_{\min} = 0.9835$, $r_{\max} = 2.9532$. We used 30 and 120 lattice sites for **(a)** and **(b)** respectively, the large number in the latter necessary for demonstrating excellent convergence in all the branches.

V. DESIGN OF GENERIC SPECTRA FROM ELECTROSTATICS

While most of this work is focused on the engineering of new classes of model Hamiltonians with real spectra, our approach is equally useful for obtaining those with desired non-real spectra of any shape, since the electrostatics analogy remains valid for PBC or OBC spectra, i.e., boundary potentials of any shape. We hereby describe two additional applications, where only certain branches of the OBC spectra need to be real.

A. Hamiltonians with real spectral branch

When desired states can be selectively filled, it suffices that the spectrum possesses a real branch which can be occupied, such that the reality of other branches become immaterial. Relaxing the requirement for the *entire* spectrum to be real greatly enlarges the space of candidate Hamiltonians. Shown in Fig. 4a, for instance, is

a simple example where the stipulated real OBC branch $x \in (0, 1.9)$ lies within a lobe-shaped stipulated PBC loop parametrized by

$$E(t) = e^{it} + e^{-2it}, \qquad |t| < \pi/3. \tag{10}$$

Considered in isolation, the reconstructed Hamiltonian would have required many non-local terms due to the cusp in the PBC loop. However, if this PBC lobe and real OBC branch were part of the full 3-fold symmetric spectrum (faded in Fig. 4a), the solution to $E(k)$ would be simply given by the expression of $E(t)$ above.

B. Multi-component Hamiltonians

With this example in mind, we can repeat our methodology for more sophisticated multi-component models. Here, the entire stipulated OBC spectra is not restricted to the real line. For definiteness, suppose we desire to have *both* the OBC and PBC spectra exhibit approximately straight line segments, such that we can get various real spectra sectors upon suitable energy translation or rotation. In Fig. 4b, the stipulated OBC spectrum is given 6 straight line segments

$$r_{\min} \leq |z| \leq r_{\max}, \qquad \arg(z) = \frac{n\pi}{3}, n \in \mathbb{Z}, \tag{11}$$

related by $\pi/3$ rotations, together with a zero mode, while the stipulated PBC spectrum is parametrized by

$$E^2(t) = ae^{-it} + e^{2it}, \tag{12}$$

which is a sixfold rotationally symmetric figure with approximately straight sides when $a = 10$. It should be noted that this t parametrization will not correspond to the expected PBC dispersion relation $E(k)$ of the engineered Hamiltonian, since only the locus of points needs to be matched.

From the geometric symmetry of the spectra, we chose a 3-component ansatz for the engineered Hamiltonian of the form

$$H_{\text{6-fold}}(k) = \begin{pmatrix} \Delta & f(k) & 0 \\ 0 & \Delta & 1 \\ 1 & 0 & \Delta \end{pmatrix}, \tag{13}$$

with dispersion $E(k) = \Delta + e^{2\pi i n/3}\sqrt[3]{f(k)}$, $n = 0, 1, 2$, such that $f(k)$ can be found from the truncated Fourier transform of the reconstructed $(E(k)-\Delta)^3$ obtained from our induced electrostatic charge solutions. For Fig. 4b, we have set the energy shift Δ to be zero; we could have set $\Delta = 3i$ had we wanted to have a segment of approximately real PBC spectrum. As shown, keeping only hoppings within the same unit cell and across 3 unit cells in $f(k)$ (see the Supplementary materials Section VI), the reconstructed spectra agree with the stipulated spectra almost perfectly. This would not have been possible had we chosen another ansatz that involves some root of $f(k)$ other than $\sqrt[3]{f(k)}$.

VI. DISCUSSION AND CONCLUSION

In a handful of memorable pages on electrostatic analogs and the unity of nature [64], Richard Feynman pointed out how many different phenomena in physics can all be explained using the equations of electrostatics. These include the heat flow between plates held at different temperatures, the vibrations of a drumhead, the diffusion of neutrons and the flow of a fluid past a sphere. Here we unravelled a new electrostatics analogy from non-Hermitian condensed matter physics and inverse quantum engineering. Specifically, we rigorously prove that the seemingly hard problem to synthesize non-Hermitian spectra in tight-binding lattices with modified bulk-boundary correspondence can be mapped onto a simple electrostatic problem. The working principle behind this analogy is the intimate relation between the conformal structure of electrostatics and the complex spectral flow in non-Hermitian systems. Our work opens up a new paradigm for engineering non-Hermitian spectra, particularly real spectra, in various settings, such as cold atoms [57, 58], photonics [24, 28], metamaterials [65, 66], mechanical and acoustic systems [60]. While real spectra are important for state stability in the majority of experiments, we point out that non-real spectra present further possibilities in terms of topological sophistication [43, 67], and are just as physically relevant in the form of the Laplacian spectra of steady-state networks such as electrical circuits [35, 63, 68–70].

Our approach will impact the design of non-Hermitian sensors [71] in optics and electronics. As finite-sized devices, they are OBC systems, and the requisite sensing properties would specify the non-Hermitian skin state profiles, which correspond to the potential profile of the analog electrostatic charges. Such sensors may find applications in measuring glucose concentrations [72] and wireless sensors [73].

Besides its versatility in discovering new classes of stable non-Hermitian Hamiltonians, our electrostatics analogy also allows numerical access to non-Hermitian lattices of far larger system sizes. Till now, the numerical computation of OBC skin spectra have been limited by rapidly compounding floating point errors, which limit accurate diagonalization results to systems smaller than $\mathcal{O}(10^2)$ sites at standard machine precision. Analytic results only exists for a small subset of systems where the generalized Brillouin zone is not excessively complicated. However, our electrostatics approach trades this non-Hermitian diagonalization problem with a boundary-value partial differential equation problem, whose numerical solution do not suffer from non-Hermitian sensitivity at all, and can be extended even towards the thermodynamic limit.

VII. CONFLICT OF INTEREST

The authors declare that they have no conflict of interest.

VIII. ACKNOWLEDGEMENTS

This work is supported by Singapore's MOE Tier I grant WBS no. A-800022-00-00.

IX. AUTHOR CONTRIBUTIONS

Ching Hua Lee developed the electrostatics analogy and initiated the project. Ching Hua Lee and Russell Yang led the project. Jun Wei Tan performed the spectral reconstruction. Russell Yang, Jun Wei Tan, Tommy Tai, and Jin Ming Koh performed the numerical computations. Stefano Longhi generalized the electrostatics analogy to point charges. Stefano Longhi, Linhu Li, and Ching Hua Lee also took on advisory roles. All authors contributed to the writing of the manuscript.

[1] C. M. Bender, D. C. Brody, and H. F. Jones, "Complex extension of quantum mechanics," *Phys. Rev. Lett.*, vol. 89, p. 270401, Dec 2002.

[2] K. Ding, G. Ma, M. Xiao, Z. Q. Zhang, and C. T. Chan, "Emergence, coalescence, and topological properties of multiple exceptional points and their experimental realization," *Phys. Rev. X*, vol. 6, p. 021007, Apr 2016.

[3] H. Hodaei, A. U. Hassan, S. Wittek, H. Garcia-Gracia, R. El-Ganainy, D. N. Christodoulides, and M. Khajavikhan, "Enhanced sensitivity at higher-order exceptional points," *Nature*, vol. 548, pp. 187–191, Aug 2017.

[4] B. Zhen, C. W. Hsu, Y. Igarashi, L. Lu, I. Kaminer, A. Pick, S.-L. Chua, J. D. Joannopoulos, and M. Soljačić, "Spawning rings of exceptional points out of dirac cones," *Nature*, vol. 525, pp. 354–358, Sep 2015.

[5] S. Yao and Z. Wang, "Edge states and topological invariants of non-hermitian systems," *Phys. Rev. Lett.*, vol. 121, p. 086803, Aug 2018.

[6] C. H. Lee and R. Thomale, "Anatomy of skin modes and topology in non-hermitian systems," *Phys. Rev. B*, vol. 99, p. 201103, May 2019.

[7] F. Song, S. Yao, and Z. Wang, "Non-hermitian skin effect and chiral damping in open quantum systems," *Physical review letters*, vol. 123, no. 17, p. 170401, 2019.

[8] K. Yokomizo and S. Murakami, "Non-bloch band theory of non-hermitian systems," *Phys. Rev. Lett.*, vol. 123, p. 066404, Aug 2019.

[9] T. Tai and C. H. Lee, "Zoology of non-hermitian spectra and their graph topology," *arXiv preprint arXiv:2202.03462*, 2022.

[10] K. Zhang, Z. Yang, and C. Fang, "Universal non-hermitian skin effect in two and higher dimensions," *Nature communications*, vol. 13, no. 1, pp. 1–7, 2022.

[11] F. Qin, R. Shen, and C. H. Lee, "Non-hermitian squeezed polarons," *arXiv preprint arXiv:2202.10481*, 2022.

[12] L. Li, S. Mu, C. H. Lee, and J. Gong, "Quantized classical response from spectral winding topology," *Nature Communications*, vol. 12, p. 5294, Sep 2021.

[13] K. Kawabata, K. Shiozaki, M. Ueda, and M. Sato, "Symmetry and topology in non-hermitian physics," *Phys. Rev. X*, vol. 9, p. 041015, Oct 2019.

[14] K. Zhang, Z. Yang, and C. Fang, "Correspondence between winding numbers and skin modes in non-hermitian systems," *Phys. Rev. Lett.*, vol. 125, p. 126402, Sep 2020.

[15] N. Okuma, K. Kawabata, K. Shiozaki, and M. Sato, "Topological origin of non-hermitian skin effects," *Phys. Rev. Lett.*, vol. 124, p. 086801, Feb 2020.

[16] D. S. Borgnia, A. J. Kruchkov, and R.-J. Slager, "Non-hermitian boundary modes and topology," *Physical Review Letters*, vol. 124, no. 5, 2020.

[17] H. Jiang and C. H. Lee, "Filling up complex spectral regions through non-hermitian disordered chains," *Chinese Physics B*, vol. 31, no. 5, p. 050307, 2022.

[18] H.-Q. Liang, S. Mu, J. Gong, and L. Li, "Anomalous hybridization of spectral winding topology in quantized steady-state responses," *Phys. Rev. B*, vol. 105, p. L241402, Jun 2022.

[19] P.-Y. Chang, J.-S. You, X. Wen, and S. Ryu, "Entanglement spectrum and entropy in topological non-hermitian systems and nonunitary conformal field theory," *Physical Review Research*, vol. 2, no. 3, p. 033069, 2020.

[20] C. H. Lee, "Exceptional bound states and negative entanglement entropy," *Phys. Rev. Lett.*, vol. 128, p. 010402, Jan 2022.

[21] C. Lv, R. Zhang, Z. Zhai, and Q. Zhou, "Curving the space by non-hermiticity," *Nature communications*, vol. 13, no. 1, pp. 1–6, 2022.

[22] C. H. Lee and S. Longhi, "Ultrafast and anharmonic rabi oscillations between non-bloch bands," *Communications Physics*, vol. 3, p. 147, Aug 2020.

[23] C. M. Bender and S. Boettcher, "Real spectra in non-hermitian hamiltonians having p t symmetry," *Physical Review Letters*, vol. 80, no. 24, p. 5243, 1998.

[24] R. El-Ganainy, K. G. Makris, M. Khajavikhan, Z. H. Musslimani, S. Rotter, and D. N. Christodoulides, "Non-hermitian physics and pt symmetry," *Nature Physics*, vol. 14, pp. 11–19, Jan 2018.

[25] L. Feng, R. El-Ganainy, and L. Ge, "Non-hermitian photonics based on parity–time symmetry," *Nature Photonics*, vol. 11, no. 12, pp. 752–762, 2017.

[26] A. Stegmaier, S. Imhof, T. Helbig, T. Hofmann, C. H. Lee, M. Kremer, A. Fritzsche, T. Feichtner, S. Klembt, S. Höfling, I. Boettcher, I. C. Fulga, L. Ma, O. G. Schmidt, M. Greiter, T. Kiessling, A. Szameit, and R. Thomale, "Topological defect engineering and $\mathcal{PT}$ symmetry in non-hermitian electrical circuits," *Phys. Rev. Lett.*, vol. 126, p. 215302, May 2021.

[27] A. Mostafazadeh, "Pseudo-hermiticity versus symmetry: The necessary condition for the reality of the spectrum of a non-hermitian hamiltonian," *Journal of Mathematical Physics*, vol. 43, pp. 205–214, 2002.

[28] S. Longhi, "Parity-time symmetry meets photonics: A new twist in non-hermitian optics," *EPL (Europhysics Letters)*, vol. 120, no. 6, p. 64001, 2018.

[29] R. El-Ganainy, M. Khajavikhan, D. N. Christodoulides, and S. K. Ozdemir, "The dawn of non-hermitian optics," *Communications Physics*, vol. 2, p. 37, Mar 2019.

[30] J. Y. Lin, N. C. Hu, Y. J. Chen, C. H. Lee, and X. Zhang, "Line nodes, dirac points, and lifshitz transition in two-dimensional nonsymmorphic photonic crystals," *Physical Review B*, vol. 96, no. 7, p. 075438, 2017.

[31] C. E. Rüter, K. G. Makris, R. El-Ganainy, D. N. Christodoulides, M. Segev, and D. Kip, "Observation of parity–time symmetry in optics," *Nature Physics*, vol. 6, pp. 192–195, Mar 2010.

[32] J. Li, A. K. Harter, J. Liu, L. de Melo, Y. N. Joglekar, and L. Luo, "Observation of parity-time symmetry breaking transitions in a dissipative floquet system of ultracold atoms," *Nature Communications*, vol. 10, p. 855, Feb 2019.

[33] A. Regensburger, C. Bersch, M.-A. Miri, G. Onishchukov, D. N. Christodoulides, and U. Peschel, "Parity–time synthetic photonic lattices," *Nature*, vol. 488, pp. 167–171, Aug 2012.

[34] A. Ghatak, M. Brandenbourger, J. van Wezel, and C. Coulais, "Observation of non-hermitian topology and its bulk–edge correspondence in an active mechanical metamaterial," *Proceedings of the National Academy of Sciences*, vol. 117, no. 47, pp. 29561–29568, 2020.

[35] T. Helbig, T. Hofmann, S. Imhof, M. Abdelghany, T. Kiessling, L. W. Molenkamp, C. H. Lee, A. Szameit, M. Greiter, and R. Thomale, "Generalized bulk–boundary correspondence in non-hermitian topolectrical circuits," *Nature Physics*, vol. 16, pp. 747–750, Jul 2020.

[36] L. Xiao, T. Deng, K. Wang, G. Zhu, Z. Wang, W. Yi, and P. Xue, "Non-hermitian bulk–boundary correspondence in quantum dynamics," *Nature Physics*, vol. 16, no. 7, pp. 761–766, 2020.

[37] D. Zou, T. Chen, W. He, J. Bao, C. H. Lee, H. Sun, and X. Zhang, "Observation of hybrid higher-order skin-topological effect in non-hermitian topolectrical circuits," *Nature Communications*, vol. 12, no. 1, pp. 1–11, 2021.

[38] A. Mostafazadeh, "Pseudo-hermiticity versus pt symmetry: The necessary condition for the reality of the spectrum of a non-hermitian hamiltonian," *Journal of Mathematical Physics*, vol. 43, no. 1, pp. 205–214, 2002.

[39] S. Yao, F. Song, and Z. Wang, "Non-hermitian chern bands," *Physical review letters*, vol. 121, p. 136802, September 2018.

[40] N. Hatano and D. R. Nelson, "Localization transitions in non-hermitian quantum mechanics," *Physical review letters*, vol. 77, no. 3, p. 570, 1996.

[41] S. Longhi, "Tight-binding lattices with an oscillating imaginary gauge field," *Phys. Rev. A*, vol. 94, p. 022102, Aug 2016.

[42] Z. Yang, K. Zhang, C. Fang, and J. Hu, "Non-hermitian bulk-boundary correspondence and auxiliary generalized brillouin zone theory," *Phys. Rev. Lett.*, vol. 125, p. 226402, Nov 2020.

[43] C. H. Lee, L. Li, R. Thomale, and J. Gong, "Unraveling non-hermitian pumping: Emergent spectral singularities and anomalous responses," *Phys. Rev. B*, vol. 102, p. 085151, Aug 2020.

[44] L. Li, C. H. Lee, and J. Gong, "Geometric characterization of non-hermitian topological systems through the singularity ring in pseudospin vector space," *Physical Review B*, vol. 100, no. 7, p. 075403, 2019.

[45] D. Wu, J. Xie, Y. Zhou, and J. An, "Connections between the open-boundary spectrum and the generalized brillouin zone in non-hermitian systems," *Phys. Rev. B*, vol. 105, p. 045422, Jan 2022.

[46] P. Krutitskii, "The dirichlet problem for the two-dimensional laplace equation in a multiply connected domain with cuts," *Proceedings of the Edinburgh Mathematical Society*, vol. 43, no. 2, pp. 325–341, 2000.

[47] X. Zhang, G. Li, Y. Liu, T. Tai, R. Thomale, and C. H. Lee, "Tidal surface states as fingerprints of non-hermitian nodal knot metals," *Communications Physics*, vol. 4, no. 1, pp. 1–10, 2021.

[48] L. Li and C. H. Lee, "Non-hermitian pseudo-gaps," *Science Bulletin*, vol. 67, no. 7, pp. 685–690, 2022.

[49] J. Feinberg and A. Zee, "Non-hermitian random matrix theory: Method of hermitian reduction," *Nuclear Physics B*, vol. 504, no. 3, pp. 579–608, 1997.

[50] H. J. Sommers, A. Crisanti, H. Sompolinsky, and Y. Stein, "Spectrum of large random asymmetric matrices," *Physical review letters*, vol. 60, no. 19, p. 1895, 1988.

[51] F. Haake, F. Izrailev, N. Lehmann, D. Saher, and H.-J. Sommers, "Statistics of complex levels of random matrices for decaying systems," *Zeitschrift für Physik B Condensed Matter*, vol. 88, no. 3, pp. 359–370, 1992.

[52] V. M. Alvarez, J. B. Vargas, and L. F. Torres, "Non-hermitian robust edge states in one dimension: Anomalous localization and eigenspace condensation at exceptional points," *Physical Review B*, vol. 97, no. 12, p. 121401, 2018.

[53] S. Longhi, "Non-bloch-band collapse and chiral zener tunneling," *Physical review letters*, vol. 124, no. 6, p. 066602, 2020.

[54] T. E. Lee, "Anomalous edge state in a non-hermitian lattice," *Phys. Rev. Lett.*, vol. 116, p. 133903, Apr 2016.

[55] L. He and D. Vanderbilt, "Exponential decay properties of wannier functions and related quantities," *Physical Review Letters*, vol. 86, no. 23, p. 5341, 2001.

[56] C. H. Lee and P. Ye, "Free-fermion entanglement spectrum through wannier interpolation," *Phys. Rev. B*, vol. 91, p. 085119, Feb 2015.

[57] R. Bouganne, M. B. Aguilera, A. Ghermaoui, J. Beugnon, and F. Gerbier, "Anomalous decay of coherence in a dissipative many-body system," *Nature Physics*, vol. 16, no. 1, pp. 21–25, 2020.

[58] W. Song, W. Sun, C. Chen, Q. Song, S. Xiao, S. Zhu, and T. Li, "Breakup and recovery of topological zero modes in finite non-hermitian optical lattices," *Physical review letters*, vol. 123, no. 16, p. 165701, 2019.

[59] R. El-Ganainy, M. Khajavikhan, D. N. Christodoulides, and S. K. Ozdemir, "The dawn of non-hermitian optics," *Communications Physics*, vol. 2, no. 1, pp. 1–5, 2019.

[60] C. Scheibner, W. T. M. Irvine, and V. Vitelli, "Non-hermitian band topology and skin modes in active elastic media," *Phys. Rev. Lett.*, vol. 125, p. 118001, Sep 2020.

[61] Q. Liang, D. Xie, Z. Dong, H. Li, H. Li, B. Gadway, W. Yi, and B. Yan, "Observation of non-hermitian skin effect and topology in ultracold atoms," 2022.

[62] Y. Gu, C. H. Lee, X. Wen, G. Y. Cho, S. Ryu, and X.-L. Qi, "Holographic duality between (2+ 1)-dimensional quantum anomalous hall state and (3+ 1)-dimensional topological insulators," *Physical Review B*, vol. 94, no. 12, p. 125107, 2016.

[63] P. M. Lenggenhager, A. Stegmaier, L. K. Upreti, T. Hofmann, T. Helbig, A. Vollhardt, M. Greiter, C. H. Lee, S. Imhof, H. Brand, *et al.*, "Electric-circuit realization of a hyperbolic drum," *arXiv preprint arXiv:2109.01148*, 2021.

[64] R. Feynman, R. Leighton, and M. Sands, *The Feynman Lectures on Physics*, vol. 2. Addison-Wesley Pub. Co, 1963.

[65] J. Hou, Z. Li, X.-W. Luo, Q. Gu, and C. Zhang, "Topological bands and triply degenerate points in non-hermitian hyperbolic metamaterials," *Phys. Rev. Lett.*, vol. 124, p. 073603, Feb 2020.

[66] L. Pickup, H. Sigurdsson, J. Ruostekoski, and P. Lagoudakis, "Synthetic band-structure engineering in polariton crystals with non-hermitian topological phases," *Nature communications*, vol. 11, no. 1, pp. 1–8, 2020.

[67] B. Zhang, Q. Li, X. Zhang, and C. H. Lee, "Real non-hermitian energy spectra without any symmetry," *Chinese Physics B*, 2022.

[68] J. Ningyuan, C. Owens, A. Sommer, D. Schuster, and J. Simon, "Time-and site-resolved dynamics in a topological circuit," *Physical Review X*, vol. 5, no. 2, p. 021031, 2015.

[69] C. H. Lee, S. Imhof, C. Berger, F. Bayer, J. Brehm, L. W. Molenkamp, T. Kiessling, and R. Thomale, "Topolectrical circuits," *Communications Physics*, vol. 1, p. 39, Jul 2018.

[70] C. Shang, S. Liu, R. Shao, P. Han, X. Zang, X. Zhang, K. N. Salama, W. Gao, C. H. Lee, R. Thomale, *et al.*, "Experimental identification of the second-order non-hermitian skin effect with physics-graph-informed machine learning," *arXiv preprint arXiv:2203.00484*, 2022.

[71] M.-A. Miri and A. Al, "Exceptional points in optics and photonics," *Science*, vol. 363, no. 6422, p. eaar7709, 2019.

[72] Y. J. Zhang, H. Kwon, M.-A. Miri, E. Kallos, H. Cano-Garcia, M. S. Tong, and A. Alu, "Noninvasive glucose sensor based on parity-time symmetry," *Phys. Rev. Applied*, vol. 11, p. 044049, Apr 2019.

[73] C. Zeng, K. Zhu, Y. Sun, G. Li, Z. Guo, J. Jiang, Y. Li, H. Jiang, Y. Yang, and H. Chen, "Ultra-sensitive passive wireless sensor exploiting high-order exceptional point for weakly coupling detection," *New Journal of Physics*, vol. 23, p. 063008, jun 2021.

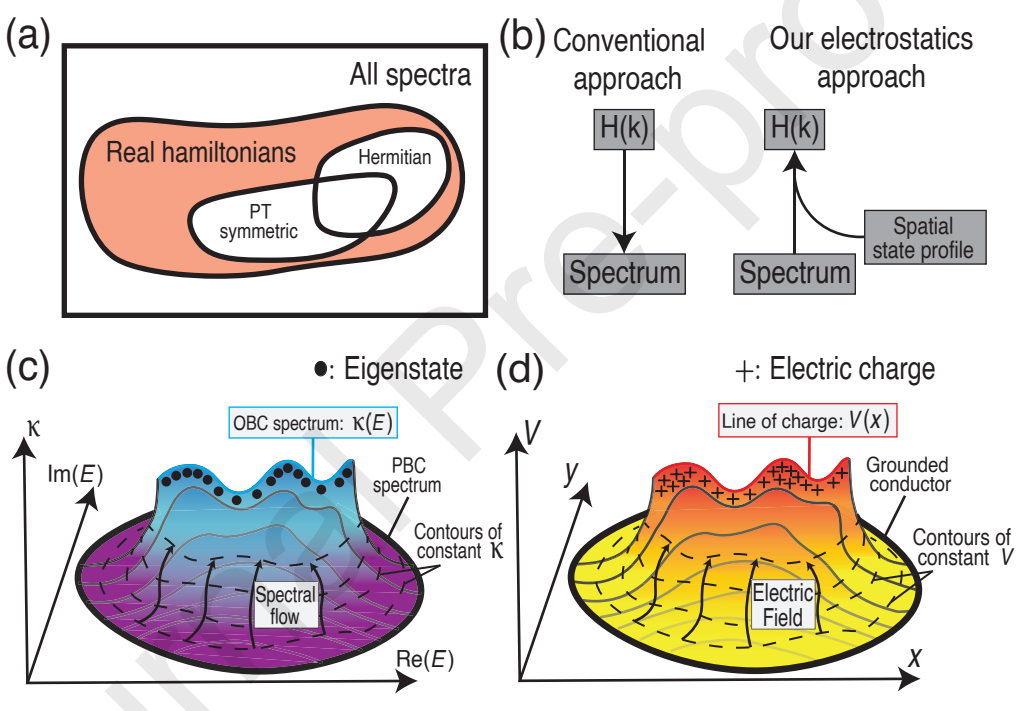
(a)
All spectra
Real hamiltonians
Hermitian
PT
symmetric
(b)
Conventional
approach
H(k)
Spectrum
Our electrostatics
approach
H(k)
Spectrum
Spatial
state profile
(c)
•: Eigenstate
κ
Im(E)
OBC spectrum: κ(E)
PBC
spectrum
Contours of
constant κ
Spectral
flow
Re(E)
(d)
+: Electric charge
V
y
Line of charge: V(x)
Grounded
conductor
Contours of
constant V
Electric
Field
x